UDC 621.315.592

Band structure of lateral plasmonic crystal tuned with magnetic field*

© I.V. Gorbenko, V.Yu. Kachorovskyi

Ioffe Institute, 194021 St. Petersburg, Russia

E-mail: gorbenko.ilya.v@gmail.com

Received April 19, 2024
Revised May 14, 2024
Accepted May 14, 2024

The transmission of terahertz radiation through a two-dimensional electron gas with a lattice gate placed in a perpendicular magnetic field B was studied. It is shown that a voltage applied to the gate creates a lateral plasma crystal with a band structure that can be controlled by both the gate voltage and the magnetic field. It has been demonstrated that only part of the lateral plasma crystal plasmonic modes is present in the transmission spectrum of homogeneous excitation, while the other half—dark modes—appear only in the case of inhomogeneous excitation. The transition between weak coupling and strong coupling regimes, as the density modulation depth changes, is theoretically described. Two excitation regimes are predicted, resonant and „super-resonant“and the transition between them is described as the quality factor of the structure increases. The main focus are the effects associated with the presence of a magnetic field. In particular, it is shown that plasmon resonances, which are visible in the transmission spectrum, approach each other with increasing of magnetic field and in the presence of a finite momentum relaxation rate can merge.

Keywords: two-dimensional electron liquid, plasma waves, dark modes, homogeneous excitation, band structure, plasmonic crystal, magnetic field, weak and strong coupling.

DOI: 10.61011/SC.2024.03.58834.6311H

1. Introduction

The possibility of detection and generation of terahertz (THz) radiation using plasma waves propagating in the simplest gate system — field effect transistor (FET) was first discussed by Dyakonov and Shur [1]. It was shown that FET is capable of converting THz radiation into direct current (dc) and, conversely, direct current can excite plasma oscillations under suitable boundary conditions. Later it turned out that multi-gate devices have a better application potential (see [3,4] and references in these papers), since plasma waves in them interact much better with THz radiation than in single FETs. Thus, the lattice gate acts as an antenna, modulating the external field. The second function of the lattice gate is the modulation of the electron density. Namely, the electronic concentration is periodically modulated in one of the directions. As a result, the spectrum of plasma excitations, similar to the spectrum of a 1D crystal, contains allowed bands and band gaps. The key advantage of the lateral plasma crystal (LPC) is the tunability of the zone structure using gate electrodes.

Despite the fact that the idea of creating a LPC was previously discussed (see, for example, Ref. [3,4] and references in them), experimental confirmation of the possibility of controlling its band structure appeared only in 2023 [5]. Plasmonic resonances of the transmission coefficient of (T) THz radiation through a GaN/AlGaN-based LPC were studied. The gate voltages determined the modulation strength and ensured the transition from the weak coupling mode (weak periodic density modulation) to the strong coupling mode (strong modulation). A theoretical model describing such a transition is constructed [6]. We theoretically show in this paper that the LPC zones can also be effectively controlled by a magnetic field. The merging of plasmon zones with an increase of the magnetic field is the key result, which can be directly experimentally verified (see Figure 1 for the dissipation density, which is proportional to $\delta T = 1-T$, depending on the radiation frequency and cyclotron frequency at different values of the momentum relaxation time).

2. Problem statement and general approach

The simplest model of a lateral plasma crystal (Figure 2) consists of alternating regions *1* and *2* with different electron concentrations and, consequently, with different plasma wave velocities, s_1 and s_2, respectively [3] (see also the discussion of various LPC geometries in the review [7]). For certainty, we will assume that $s_1 > s_2$ and, according to Ref. [8], call the area *1* as the active area, and the area *2* as the passive area (meaning of the terms „active“ and „passive“ will be explained further).

The transmission ratio T in the case of linearly polarized light can be written using a simple formula [8]

$$T \approx 1 - \frac{P}{S}, \tag{1}$$

where P — radiation dissipation, $S = c\sqrt{\varepsilon}E_0^2/8\pi e^2$ — time-averaged Poynting vector, E_0 — amplitude of external

* XXVIII International Symposium „Nanophysics and Nanoelectronics“, Nizhny Novgorod, 11—15 March 2024

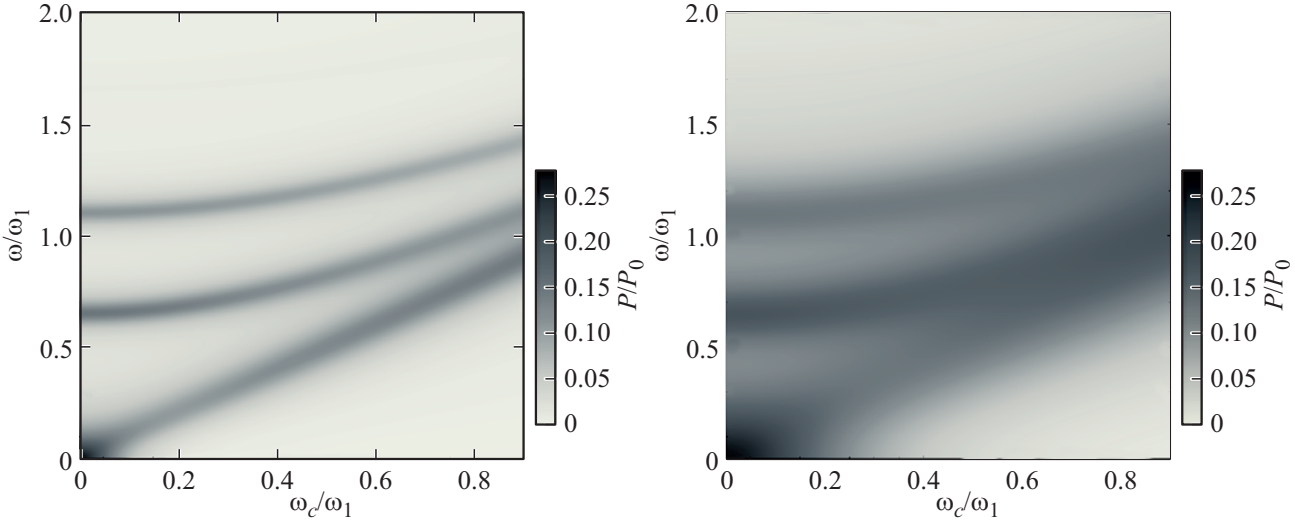

Figure 1. Heatmap P/P_0 in the plane $(\omega/\omega_1, \omega_c/\omega_1)$ at $\gamma = 0.1\omega_1$ (top) and $\gamma = 0.3\omega_1$ (bottom), $s_2 = 0.4s_1$, $L_2 = L_1$. The transition from a super-resonance mode to a resonant mode with an increase of γ and (or) ω_c is clearly visible in the form of a resonance overlap. $P_0 = F_0^2 N_1/2m\gamma$.

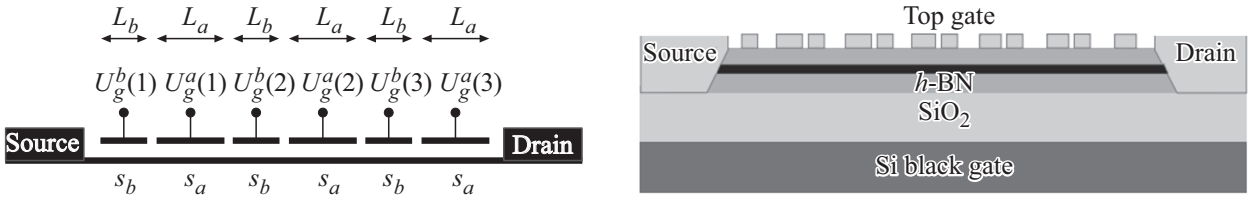

Figure 2. Some configurations of the lateral plasma crystal: a structure with several gates that are offset so that the potential difference between the gate and the channel has translational symmetry (figure on the left from Ref. [3]), a schematic representation of the device in cross section with an asymmetric double metal lattice (figure on the right from Ref. [8]).

radiation, c — speed of light, e — electron charge, ε — dielectric constant.

Thus, it is necessary to calculate the radiation dissipation P for finding the transmission coeffitient T. We search for the radiation-induced velocity and calculate the local ohmic dissipation per unit length, which in the hydrodynamic approximation is given by [8,9]:

$$P \approx \frac{mN_0}{\tau} \langle |\mathbf{v}|^2 \rangle_{x,t}, \tag{2}$$

where N_0 — constant electron concentration in the channel, $n = (N - N_0)/N_0$ — dimensionless radiation-induced concentration, $\mathbf{v}(x, t)$ — electron liquid velocity, τ — pulse relaxation time. The coordinate averaging is carried out along the cell of the lateral crystal.

3. Hydrodynamic approximation

We assume that electron-electron collisions determine the basic properties of the system, and describe the electron liquid in the channel by hydrodynamic equations — the Navier-Stokes equation, including the Lorentz force, and the continuity equation:

$$\frac{\partial \mathbf{v}}{\partial t} + (\mathbf{v}\boldsymbol{\nabla})\mathbf{v} + \frac{\mathbf{v}}{\tau} = -s^2 \nabla n + [\omega_c \mathbf{v}] + \frac{\mathbf{F}}{m}, \tag{3}$$

$$\frac{\partial n}{\partial t} + \mathrm{div}(n\mathbf{v}) = 0. \tag{4}$$

Here ω_c — cyclotron frequency, m — effective electron mass, $s = s_{1,2}$ — plasma velocity. The external force is directed along the axis X: $F(t) = eE_0 \cos \omega t$, which sets the external homogeneous radiation, the term $-s^2 \nabla n$ determines the acceleration associated with the concentration gradient. The modulation of the gate array of external radiation is discussed in Ref. [6].

We linearize the Navier-Stokes and continuity equations (3), (4), substituting the solution in the form $\{\delta n, vx, vy\} \propto \exp(iqx - i\omega t) + \text{c.c.}$:

$$\begin{gathered} (\gamma - i\omega)v_x - \omega_c v_y + iqs^2 \delta n = F_0/2m, \\ \omega_c v_x + (\gamma - i\omega)v_y = 0, \\ iqv_x - i\omega\delta n = 0. \end{gathered} \tag{5}$$

It should be noted from here that

$$|\mathbf{v}(x)|^2 = |v_x|^2 + |v_y|^2 = \left(1 + \frac{\omega_c^2}{\omega^2 + \gamma^2}\right)|v_x|^2. \tag{6}$$

The LPC consists of alternating bands with plasma wave velocities s_1 and s_2 and corresponding lengths L_1 and L_2. Standard boundary conditions are applied at the boundaries [3,6] corresponding to the conservation of current and energy flow at the boundary between the stripes (we assume that there is no direct current in the channel):

$$s^2\delta n = \text{const}, \quad s^2 v_x = \text{const}. \tag{7}$$

Next, taking into account the equations (2) and (6) we obtain an expression with explicit coordinate averaging, divided by LPC regions:

$$P = \frac{2m\gamma}{L_1+L_2}\left(1+\frac{\omega_c^2}{\omega^2+\gamma^2}\right) \times \left[N_1 \int_0^{L_1} \langle |v_x|^2\rangle_t \, dx + N_2 \int_{L_1}^{L_1+L_2} \langle |v_x|^2\rangle_t \, dx\right]. \tag{8}$$

The following is obtained as a result of calculations

$$P = \left(1+\frac{\omega_c^2}{\omega^2+\gamma^2}\right)\frac{E_0^2 C\gamma\omega^2}{2(L_1+L_2)(\Omega^2+\Gamma^2)^2} \times \left[(L_1 s_1^2 + L_2 s_2^2) + \frac{(s_1^2-s_2^2)\,\mathrm{Re}[(\Gamma - i\Omega)\Sigma]}{\Omega\Gamma(\Gamma^2+\Omega^2)|\Sigma|^2}\right], \tag{9}$$

where the resonant frequencies are determined by the parameter $\Sigma = s_1 \cot q_1 L_1/2 + s_2 \cot q_2 L_2/2$, C — channel capacity per unit area, $\gamma = \tau^{-1}$. The heat map P/P_0 in the plane $(\omega/\omega_1, \omega_c/\omega_1)$ is shown in Figure 1.

The wave vector $q_{1,2} = (\Omega + i\Gamma)/s_{1,2}$ is determined by the real parameters Ω and Γ:

$$\Omega + i\Gamma = \sqrt{\omega\,\frac{(\omega+i\gamma)^2-\omega_c^2}{(\omega+i\gamma)}}.$$

The formula (9) is the main analytical result of this study.

4. Resonant frequencies

We fix the speed s_1, assuming that the parameter s_2 changes in the range from 0 to s_1. If $s_1 - s_2 \ll s_1$, then plasma waves propagate in an almost homogeneous system with weak scattering at the boundaries between the regions *1* and *2*. We call this case the weak coupling mode (Figure 3). The opposite case corresponds to the complete depletion of the region *2*, i. e., the zero velocity of the plasmon in this region, $s_2 = 0$. In this case, the system is divided into a set of well-conducting strips with plasma velocity s_1, separated by insulating regions. At the same time, plasma oscillations in various conductive stripes are not connected in any way. Next, we will call this case the strong coupling mode (Figure 3). A band structure is formed in pure ballistic LPC systems, where the plasmon lifetime is sufficiently long, which can appear in an experiment.

Figure 3. Switching from strong coupling mode to weak coupling mode as the parameter s_2/s_1 increases.

We found natural frequencies of the lateral PC in this study and compare them with the resonant dissipation frequencies P. The band structure of the ideal PC (at $\gamma = 0$) can be found using the Kronig–Penny model:

$$\cos[K(L_1+L_2)] = \cos\frac{\pi\Omega}{\omega_1}\cos\frac{\pi\Omega}{\omega_2} - \frac{s_1^2+s_2^2}{2s_1s_2}\sin\frac{\pi\Omega}{\omega_1}\sin\frac{\pi\Omega}{\omega_2}, \tag{10}$$

where $\Omega = \sqrt{\omega^2-\omega_c^2}$, $\omega = \omega(K)$ — the natural frequency of the plasmon, $\omega_1 = \pi s_1/L_1$ and $\omega_2 = \pi s_2/L_2$ — the frequencies of „active“ and „passive“ regions, K — quasi-momentum of a plasma crystal. The equation (10) for $\omega_c = 0$ coincides with the spectrum found in Ref. [3]. Considering the normal incidence of external radiation, the natural frequencies of plasma waves in the PC can be searched for as solutions to the equation (10) with $K = 0$. Then the equation can be written as a product of $Q_{\text{bright}}(\Omega)Q_{\text{dark}}(\Omega) = 0$, where

$$Q_{\text{bright}} = s_1 \cos\frac{\pi\Omega}{2\omega_1}\sin\frac{\pi\Omega}{2\omega_2} + s_2\cos\frac{\pi\Omega}{2\omega_2}\sin\frac{\pi\Omega}{2\omega_1},$$

$$Q_{\text{dark}} = s_2 \cos\frac{\pi\Omega}{2\omega_1}\sin\frac{\pi\Omega}{2\omega_2} + s_2\cos\frac{\pi\Omega}{2\omega_2}\sin\frac{\pi\Omega}{2\omega_1}.$$

It should be noted that the resonant frequencies ω_n, defined by $\Sigma(\omega_n, \gamma = 0) = 0$, also satisfy the equation $Q_{\text{bright}}(\omega_n) = 0$. Thus, only light modes are optically excited, and $Q_{\text{dark}}(\omega_n) \neq 0$. Solutions describing dark modes $\omega_n^{\text{dark}} : Q_{\text{dark}}(\omega_n^{\text{dark}}) = 0$ do not appear in the dissipation of a homogeneous field, unlike the light modes.

5. Weak and strong coupling regime

The equation (9) is valid for an arbitrary value of the parameter $s_2/s_1 \in [0;1]$, thus describing the transition between weak and strong coupling regimes. The resonant regime will be discussed in this section, while the nonresonant regime is discussed in detail in Ref. [10].

Next, we will consider the weak and strong coupling regimes, before entering the parameter

$$\gamma_n(\omega, \omega_c) = \gamma\,\frac{\omega^2+2\omega_c^2}{\omega^2+\omega_c^2} = \begin{cases}\gamma & \omega_c \ll \omega \\ 2\gamma & \omega_c \gg \omega\end{cases}.$$

The expression (9) is simplified in the strong coupling regime, when $s_2 \ll s_1$, under the condition of the resonant regime $\omega_2 \ll \gamma \ll \omega_1$:

$$P^{\text{strong}} = P_0 \sum_{n=0}^{\infty} \frac{\gamma\gamma_n B_n}{(\delta\omega_n^{\text{strong}})^2 + \gamma_n^2/4},$$

where

$$B_n = \frac{2L_1}{(L_1+L_2)(1+2n)^2\pi^2},$$

$$\delta\omega_n^{\text{strong}} = \omega - \sqrt{(\omega_n^{\text{strong}})^2 + \omega_c^2},$$

$$\omega_n^{\text{strong}} = \omega_1(2n+1), \quad \gamma_n = \gamma_n(\omega_n^{\text{strong}}, \omega_c).$$

The expression (9) has the following form in the weak coupling regime, when $s_2 \approx s_1$, and under the condition of super-resonant regime, when $\gamma \ll \omega_1, \omega_2$

$$P^{\text{weak}} = P_0 \sum_{n=0}^{\infty} \frac{\gamma\gamma_n A_n}{(\delta\omega^{\text{weak}})^2 + \gamma_n^2/4},$$

where

$$A_n = \frac{4(s_1-s_2)^2\left(1-(-1)^n\cos[nk(L_1-L_2)/2]\right)}{(\omega_n^{\text{weak}})^2(L_1+L_2)^2},$$

$$\delta\omega_n^{\text{weak}} = \omega - \sqrt{(\omega_n^{\text{weak}})^2 + \omega_c^2},$$

$$\omega_n^{\text{weak}} = ks_1 n, \quad \gamma_n = \gamma_n(\omega_n^{\text{weak}}, \omega_c).$$

6. Conclusion

The heat dissipation map (and, simultaneously, the transmission ratio map, see equation (1)) is shown in Figure 4 for fixed $\omega_{1,2}$ and different values γ. As can be seen, the resonant frequencies increase as $\sqrt{\omega_n^2 + \omega_c^2}$ with an increase of the magnetic field, and the gap between neighboring resonances decreases. Thus, the magnetic field takes the system out of the super-resonance mode (when all solutions of ω_n are distinguishable) into the resonant mode (when $\omega_{n+1} - \omega_n \sim \gamma$).

In addition, the difference between plasmonic resonance and cyclotron frequency decreases with the magnetic field, so that for large magnetic fields, plasmonic and cyclotron resonances overlap due to the finite attenuation γ and become indistinguishable.

Funding

This study was supported by grant No. 20-12-00147-P from the Russian Science Foundation. The work of I.G. was also supported by a grant from the foundation „BASIS“.

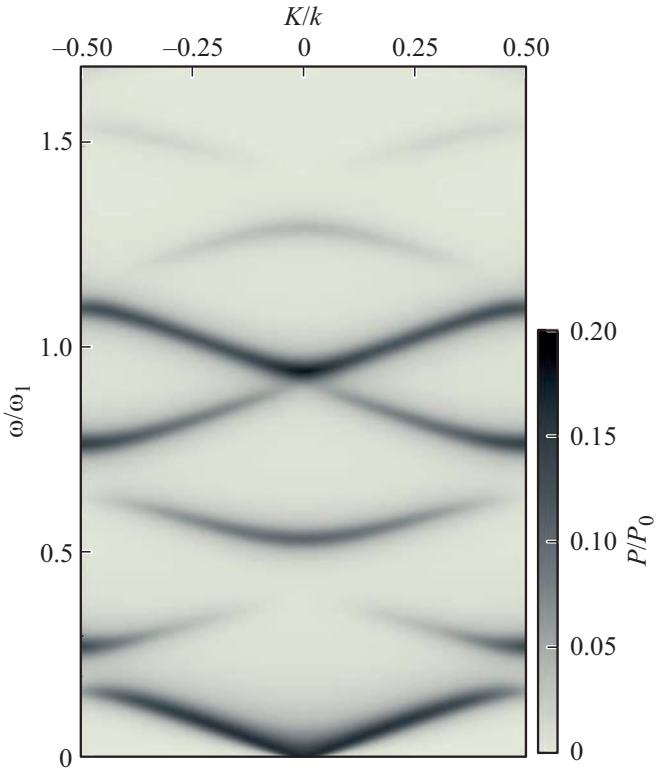

Figure 4. Heat map P/P_0 in the plane $(K/k, \omega/\omega_1)$ at $\gamma = 0.05\omega_1$. $s_2 = 0.3s_1$, $L_2 = L_1$, $k = 2\pi/(L_1+L_2)$ — inverse lattice vector. The details of the calculation are presented in Ref. [6]. This figure clearly shows how the case $K \neq 0$ excites dark modes breaking the symmetry of the problem.

References

[1] M. Dyakonov, M. Shur. Phys. Rev. Lett., **71**, 2465 (1993).
[2] M. Dyakonov, M. Shur. IEEE Trans. Electron Dev., **43**, 380 (1996).
[3] V.Yu. Kachorovskii, M.S. Shur. Appl. Phys. Lett., **100**, 232108 (2012).
[4] A.S. Petrov, D. Svintsov, V. Ryzhii, M.S. Shur. Phys. Rev. B, **95**, 045405 (2017).
[5] P. Sai, V.V. Korotyeyev, M. Dub, M. Słowikowski, M. Filipiak, D.B. But, Yu. Ivonyak, M. Sakowicz, Yu.M. Lyaschuk, S.M. Kukhtaruk, G. Cywiński, W. Knap. Phys. Rev. X, **13**, 041003 (2023).
[6] I.V. Gorbenko, V.Yu. Kachorovskii. arXiv:2401.08826 (2024).
[7] M. Shur, G. Aizin, T. Otsuji, V. Ryzhii. Sensors, **21**, 7907 (2021).
[8] S. Boubanga-Tombet, W. Knap, D. Yadav, A. Satou, D. But, V. Popov, I. Gorbenko, V. Kachorovskii, T. Otsuji. Phys. Rev. X, **10**, 031004 (2020).
[9] I.V. Rozhansky, V.Y. Kachorovskii, M.S. Shur. Phys. Rev. Lett., **114**, 246601 (2015).
[10] I.V. Gorbenko, V.Yu. Kachorovskii. arXiv:2405.06441 (2024).

Translated by A.Akhtyamov